

A search for massive young stellar objects towards 98 CH₃OH maser sources

Tie Liu, Yue-Fang Wu * and Ke Wang

Department of Astronomy, Peking University, Beijing 100871, China

Abstract Using the 13.7 m telescope of Purple Mountain Observatory (PMO), a survey of J=1-0 lines of CO and its isotopes was carried out towards 98 methanol maser sources in January 2008. Eighty-five sources have infrared counterparts within one arcmin. In the survey, except 43 sources showing complex or multiple-peak profiles, almost all the ¹³CO line profiles of the other 55 sources have large line widths of 4.5 km s⁻¹ on average and are usually asymmetric. Fifty corresponding Infrared Astronomical Satellite (IRAS) sources of these 55 sources are with L_{bol} larger than $10^3 L_{\odot}$, which can be identified as possible high-mass young stellar sources. Statistics show that the ¹³CO line widths correlate with the bolometric luminosity of the associated IRAS sources. We also report the mapping results of two sources: IRAS 06117+1350 and IRAS 07299-1651 here. Two cores were found in IRAS 06117+1350 and one core was detected in IRAS 07299-1651. The northwest core in IRAS 06117+1350 and the core in IRAS 07299-1651 can be identified as precursors of UC HII regions or high-mass protostellar objects (HMPOs). The southeast core of IRAS 06117+1350 has no infrared counterpart, seeming to be on younger stages than pre-UC HII phase.

Key words: stars: formation — ISM: clouds — ISM: methanol maser

1 INTRODUCTION

The formation and evolution of massive stars is still in mystery and our understanding of how high-mass stars form and evolve lags behind that of low-mass stars, which is understood better using the theory constructed by Shu et al. 1987. High-mass stars can produce an enormous impact on their local environment and the evolution of the whole Galaxy. However, due to their far-away location, generation in clusters and short evolutionary time scales, it is difficult to find samples of high-mass young sources to investigate their forming processes.

In the past, interstellar H₂O maser (e.g. Plume et al. 1992; Wu et al. 2006) was used as tracers for high-mass star formation regions in early evolutionary phase. However H₂O maser can also be found in low-mass star formation regions (e.g., Wu et al. 2004), while methanol (CH₃OH) masers seem to exclusively associate

with high-mass star formation regions (e.g. Minier et al. 2003). Methanol masers are traditionally divided into two classes. Class II methanol masers are found in the vicinity of the high-mass young stellar objects, while Class I methanol masers are believed to trace distant parts of the outflows from these high-mass star formation regions (Sobolev et al. 2005). With the motivation of finding more pre-UC HII regions or even more earlier high-mass stellar objects, we carried out a survey of J=1-0 lines of ^{12}CO and its isotopes ^{13}CO and C^{18}O towards 98 methanol maser sources. Next section describes the observations. Survey results and mapping results will be given and discussed in section 3. Section 4 summarizes the paper.

2 OBSERVATIONS

The observations were made in January 2008 with the 13.7 m telescope of PMO at Qinghai Station. The ^{12}CO , ^{13}CO and C^{18}O (J=1-0) lines were observed simultaneously by a superconductor receiver. The back-end is equipped with three acousto-optic spectrometers (AOSs). Every spectrometer has 1024 channels. The total bandwidths were 145.330 MHz, 42.762 MHz and 43.097 MHz for ^{12}CO , ^{13}CO and C^{18}O lines, corresponding velocity resolutions of 0.37, 0.11 and 0.12 km s^{-1} , respectively. The system temperatures during the observation ranged from 200 K to 350 K (SBD), depending on the weather. The half-power beamwidth (HPBW) at 112 GHz was $\sim 59''$. The pointing accuracy of the telescope was better than $8''$, and the main beam efficiency at the zenith was about 0.67.

We adopted the position switch mode for all the spectral measurement. Our mapping steps toward right ascension and declination directions were both 1 arcmin. The integrating time was ~ 3 minutes per position. The noise level of antenna temperature T_A^* was usually about 0.4 K for the ^{12}CO , 0.3 K for the ^{13}CO and 0.2 K for the C^{18}O (J=1-0) band, respectively. For the data analysis, the GILDAS software package including CLASS and GREG was employed (Guilloteau & Lucas 2000).

3 RESULTS AND DISCUSSION

3.1 Sample analysis

Ninety-eight sources were observed, 29 of which belong to the Class I methanol masers. Table 1 presents basic parameters of all the sources surveyed. The associated IRAS sources within a $3' \times 3'$ are presented in column 2. Eighty-five have IR counterpart candidates within one arcmin. Columns 3-6 give the equatorial coordinates and the Galactic coordinates, respectively. The color indices $\log(F_{25}/F_{12})$ and $\log(F_{60}/F_{12})$ are presented in columns 7-8 (F_{12} , F_{25} , and F_{60} represent the flux at $12\mu\text{m}$, $25\mu\text{m}$ and $60\mu\text{m}$, respectively.). Column 9 lists the fluxes at $100\mu\text{m}$. The types of these methanol masers and the related references were placed in columns 10-11.

Figure 1 shows the distribution of the sources surveyed in Galactic coordinates. The sample sources concentrate on the Galactic plane ($|b| < 2^\circ$) and about 90% are found in the first quadrant. Only the Orion's source is with $|b| > 15^\circ$, and 72 sources are located in $0 < l < 45^\circ$.

The locations of the associated IRAS sources in the color-color planes are plotted in Figure 2. The distributions show that about 75% of the Class I and 63% of the Class II methanol maser sources ob-

& Churchwell 1989. All of these UC HII region candidates except Orion's source are with flux larger than 100 Jy at 100 μm .

3.2 Survey results and discussion

All the 98 sources are detected with J=1-0 lines of the ^{12}CO , ^{13}CO and C^{18}O . Forty-three sources hold too complex line profiles and will be studied further. The other fifty-five sources were analyzed, including 17 Class I methanol maser sources. Figure 3 presents the spectra of all the 55 sources and one source IRAS 18403-0417 with blended lines. The grey, green and red lines represent ^{12}CO , ^{13}CO and C^{18}O respectively. The ^{12}CO spectra of IRAS 18414-1723, IRAS 18353-0628, G32.74-0.07 and G39.10+0.48 are blended, but the relevant ^{13}CO emission spectra can be well distinguished. So these four sources are also analyzed. In the 55 sources, we detected significant ^{12}CO and ^{13}CO signals, but only 60% in them showed obvious C^{18}O signals. No differences are found in the detection rate of J=1-0 lines of CO isotopes between class I and class II methanol maser sources. These 55 sources present profuse ^{13}CO line profiles. About 40% of them hold wings and nearly 20 sources have more than one components. We fitted these ^{13}CO lines with a Gaussian function. We distinguish between several different non-Gaussian ^{13}CO line profiles with the following characters:

(a)wings; (b)red wing; (c)blue wing; (d)red shoulder; (e)red asymmetry; (f)blue asymmetry; (g)flat top; (h)two or three components.

The identities of these ^{13}CO spectra characters are presented in column 12 of Table 2. Possible clues of high velocity gas were detected in five sources of Class I and nine sources of Class II methanol maser sources (see the last column of Table 2). There seem no differences in high velocity gas detection rate between Class I and Class II methanol maser sources. Detailed investigations with denser molecular probers such as HCN and CS are needed.

Observation parameters including the antenna temperature T_A^* , V_{LSR} and ^{13}CO line width (FWHM) of each components were obtained and shown in columns 2-4 of Table 2. Columns 5-6 list the distances from the Galactic center (R) and the Sun (D). Nine components cannot provide available distances from fitting Galactic rotational curve. Column 7 presents the bolometric luminosity calculated with the formation in Casoli et al. 1986:

$$L_{(5-1000\mu m)} = 4\pi D^2 \times 1.75 \times (F_{12}/0.79 + F_{25}/2 + F_{60}/3.9 + F_{100}/9.9) \quad (1)$$

where D is the distance. Fifty of the 55 sources are with $L_{bol} > 10^3 L_{\odot}$, supposed to be massive star formation regions.

Assuming that ^{12}CO is optically thick, we derived the excited temperatures T_{ex} following Garden et al. (1991). Assuming ^{13}CO is optically thin, then the optical depth and column density of ^{13}CO can be straightforwardly obtained under local thermal equilibrium assumption (LTE). With the abundance ratio $[\text{H}_2]/[^{13}\text{CO}] = 8.9 \times 10^5$, the column density of H_2 was calculated. The results are listed in columns 8-11.

Figure 4 presents the plot of bolometric luminosity L_{bol} vs. ^{13}CO line widths of the 55 sources. The linear fit gives: $\log(L_{bol}/L_{\odot}) = 2.5 \log(\text{FWHM}/\text{km s}^{-1}) + 3.2$; the correlation coefficient $r=0.52$. From column 4 of Table 2 we can see almost all the ^{13}CO lines except one component of the source G32.74-0.07

et al.(1983). And 57 out of these 79 resolved components are with ^{13}CO line widths larger than 3 km s^{-1} , indicating possible high-mass star formation regions (Wu et al. 2003). The average line width of ^{13}CO is 4.5 km s^{-1} , similar to that detected by Purcell et al. 2009. These results indicate that sources with large line widths tend to form high-mass stars. This trend is consistent with the results of Wang et al. 2009. We also fitted the C^{18}O lines of 30 sources and found they hold line widths of 4 km s^{-1} on average, smaller than the ^{13}CO lines, respectively. The ^{13}CO lines antenna temperatures of about one half of these 30 sources are larger than 5.5 times of C^{18}O lines, and about 75% of the integrated intensities of ^{13}CO lines are larger than 5 times of C^{18}O lines, respectively. However, the center velocities of C^{18}O lines match with ^{13}CO lines very well, suggesting that ^{13}CO emissions and C^{18}O emissions may be from the same region in the cloud.

3.3 Mapping results and discussion

Two sources IRAS 06117+1350 and IRAS 07299-1651 were mapped. Figure 5 presents the contours of the integrated intensities of ^{13}CO lines. IRAS 06117+1350 has two cores and we mark them with 06117+1350-SE and 06117+1350-NW. One core was detected in IRAS 07299-1651. The positions of IRAS sources are marked with "+" and the Midcourse Space Experiment (MSX) sources are visualized with triangles.

We calculated the masses of the cores under the LTE assumption. We also calculated the virial mass using the equation from Ungerechts et al. 2000. The physical results of these cores are listed in Table 3. The two cores in IRAS 06117+1350 have virial mass smaller than the core mass, indicating they are stable and the gas motions are gravitationally bound. Specially, all of our cores are far away from UC HII regions. No Spitzer / IRAC data are available for the mapped sources. The core in IRAS 07299-1651 is with the IRAS source and three MSX sources. The northwest core of IRAS 06117+1350 is far away from any IRAS source but associated with one MSX source about $0.5'$ from the ^{13}CO emission peak. Since no 6 cm emissions associate with these two cores, they can be identified as HMPOs or UC HII precursors (e.g. Wu et al. 2006 and the references there in). The southeast core of IRAS 06117+1350 is separated from any IRAS source and MSX source, indicating an evolutionary stages earlier than pre-UC HII.

4 SUMMARY

A survey in CO and its isotopes to the locations traced by methanol masers was performed. Fifty-five sources are further studied. They all have J=1-0 emissions of ^{12}CO and ^{13}CO , but only 60% of them have significant C^{18}O emissions. No differences in both CO detection rate and high velocity gas detection rate were found between Class I and Class II methanol maser sources. Fifty of these 55 sources are associated with luminous IRAS sources ($L_{bol} > 10^3 L_{\odot}$). The relationship between the bolometric luminosity of the associated IRAS sources and ^{13}CO line widths can be well described as: $\log(L_{bol}/L_{\odot}) = 2.5\log(FWHM/km \text{ s}^{-1}) + 3.2$. About three quarters of the resolved components have ^{13}CO line widths much larger than 3 km s^{-1} . These results show that molecular cores with large line widths tend to form high-mass stellar objects. In 30 sources, ^{13}CO lines have larger line widths and antenna temperatures than C^{18}O lines. But the center velocities of C^{18}O lines match with ^{13}CO lines very well, suggesting that ^{13}CO emissions and C^{18}O emissions may be

Two cores are detected in IRAS 06117+1350 and one core in IRAS 07299-1651. The two cores in IRAS 06117+1350 have virial mass less than the core mass, but the core in IRAS 07299-1651 has virial mass larger than the core mass. The core in IRAS 07299-1651 and the northwest core of the source IRAS 06117+1350 may be pre-UC HII or HMPOs and the southeast core of IRAS 06117+1350 revealed seems to be on an earlier evolutionary stage than pre-UC HII phase.

Acknowledgements We are grateful to all the staff of Qinghai station of PMO for their assistances during the observations. N.C. Sun and Y.A. Mao are also deserved our thanks for their help and discussions. This project is supported by NSFC 10733030 and 10873019.

References

- Bachiller R., Menten, K. M., Gómez-González, J., Barcia A., 1990, *A&A*, 240, 116
- Blaszkiewicz, L., & Kus, A. J., 2004, *A&A*, 413, 233
- Casoli, F., Dupraz, C., Gerin, M., Combes, F., Boulanger, F., 1986, *A&A*, 169, 281
- Caswell, J. L., Gardner, F. F., Norris, R. P., Wellington, K. J., McCutcheon, W. H., Peng, R. S., 1993, *MNRAS*, 260, 425
- Garden, R. P., Hayashi, M., Gatley, I., Hasegawa, T., Kaifu, N., 1991, *ApJ*, 374, 540
- Guilloteau, S. & Lucas, R., 2000, in *Imaging at Radio through Submillimeter Wavelengths*, eds. J. G. Mangum., & S. Radford, *ASP Conf. Ser.*, 217, 299
- Haschick, A. D., & Baan, W. A., 1989, *ApJ*, 339, 949
- Haschick, A. D., Menten, K. M., & Baan, W. A., 1990, *ApJ*, 354, 556
- Kalenskii, S. V., Liljeström, T., Val'tts, I. E., Vasil'kov, V. I., Slysh, V. I., Urpo, S., 1994, *A&AS*, 103, 129
- Minier, V., Ellingsen, S. P., Norris, R. P., Booth, R. S., 2003, *A&A*, 403, 1095
- Myers, P., Linke, R. A., Benson, P. J., 1983, *ApJ*, 264, 517
- Plume, R., Jaffe, D. T., Evans, N. J. II, 1992, *ApJS*, 78, 505
- Purcell, C. R., Longmore, S. N., Burton, M. G., Walsh, A. J., Minier, V., Cunningham, M. R. & Balasubramanyam, R., 2009, *MNRAS*, 394, 323
- Shu, F. H., Adams, F. C., & Lizano, S., 1987, *ARA&A*, 25, 23
- Slysh, V. I., Kalenskii, S. V., Val'tts, I. E., Otrupcek, R., 1994, *MNRAS*, 268, 464
- Slysh, V. I., Val'tts, I. E., Kalenskii, S. V., Voronkov, M. A., Palagi, F., Tofani, G., Catarzi, M., 1999, *A&AS*, 134, 115
- Sobolev, A. M., et al, 2006, *arxiv:astro-ph/0601260*
- Szymczak, M., Hrynek, G., Kus A. J., 2000, *A&AS*, 143, 269
- Szymczak, M., Kus, A. J., Hrynek, G., Kepa, A., Pazderski, E., 2002, *A&A*, 392, 277
- Ungerechts, H., Umbanhowar, P., Thaddeus, P., 2000, *ApJ*, 537, 221
- Val'tts, I. E., & Condon, G. M., 2007, *Astronomy reports*, 51, 519
- Wang K., Wu Y., Ran L., Yu W., Miller M., 2009, *A&A*, 507, 369
- MNRAS*, 301, 640
- Wood, D. O. S., & Churchwell, E., 1989, *ApJ*, 340, 265
- Wu, Y., Wu, J., Wang, J., 2003, *Chinese Physics Letters*, 20, 1409
- Wu, Y., Wei, Y., Zhao, M., Shi, Y., Yu, W., Qin, S., Huang, M., 2004, *A&A*, 426, 503
- Wu, Y., Zhang, Q., Yu, W., Miller, M., Mao, R., Sun, K., Wang, Y., 2006, *A&A*, 450, 607

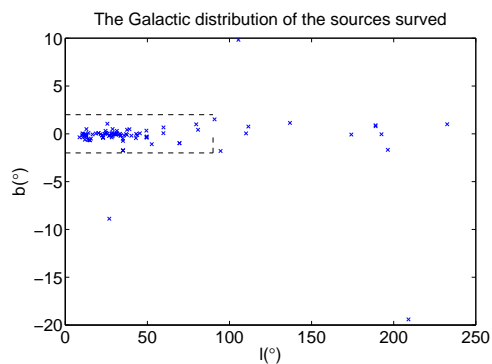


Fig. 1 The Galactic distribution of the sources surveyed. The dashed lines indicate the region with $|b| < 2^\circ$ and $0 < l < 90^\circ$. Nearly all the sources crowd to the Galactic plane, and in the longitude range 0° to 60° the plane is so densely populated.

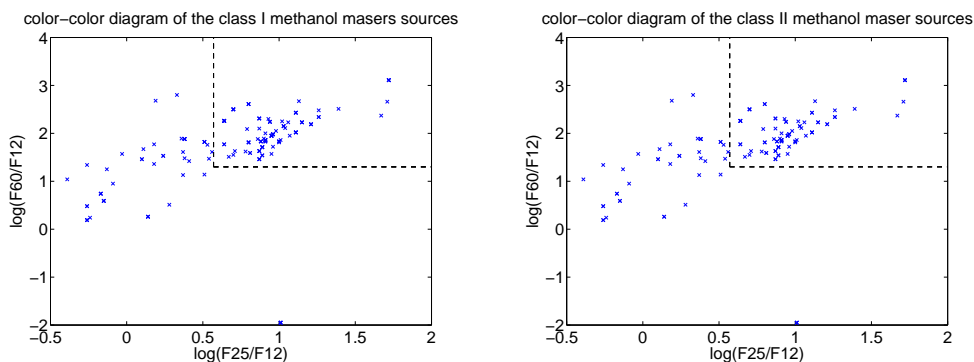


Fig. 2 The left Panel describes the color-color distribution of the 29 Class I methanol maser sources and the right Panel is for the 69 Class II methanol maser sources. The color box of UC HII regions established by Wood & Churchwell 1989 is indicated by the dashed lines in both panels.

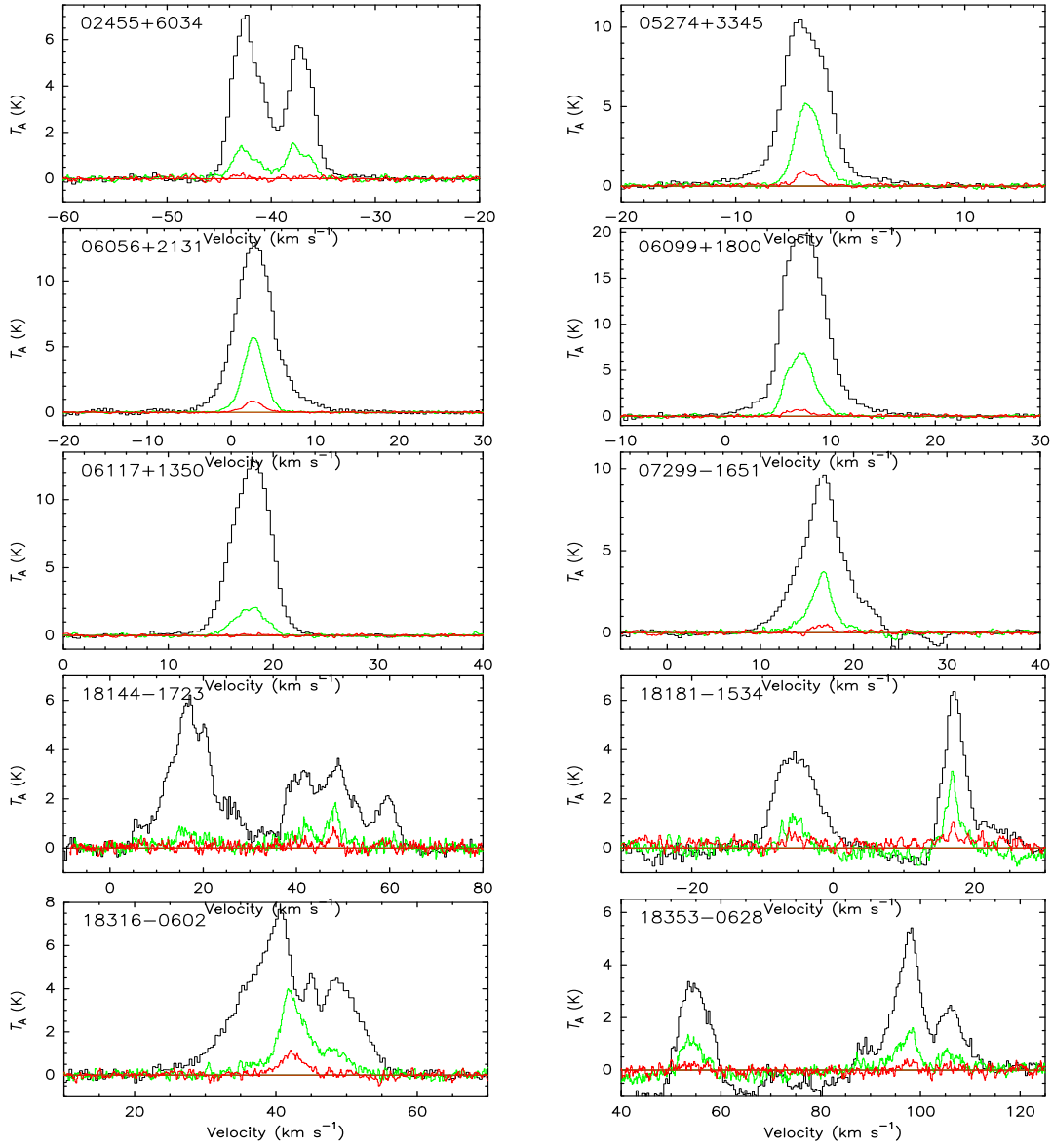


Fig. 3 Spectra of emission line samples. The grey, green and red lines represent ^{12}CO , ^{13}CO and C^{18}O $J=1-0$, respectively. The source names are drawn on the upper-left corners of each panel. The ^{12}CO spectra of IRAS 18414-1723, IRAS 18353-0628, G32.74-0.07 and G39.10+0.48 are blended, but the respect ^{13}CO emission spectra can be well distinguished. Source G29.86-0.05 is a sample with blended ^{13}CO emission lines. Properties of these ^{13}CO emission line profiles can be found in column 12 of Table 2.

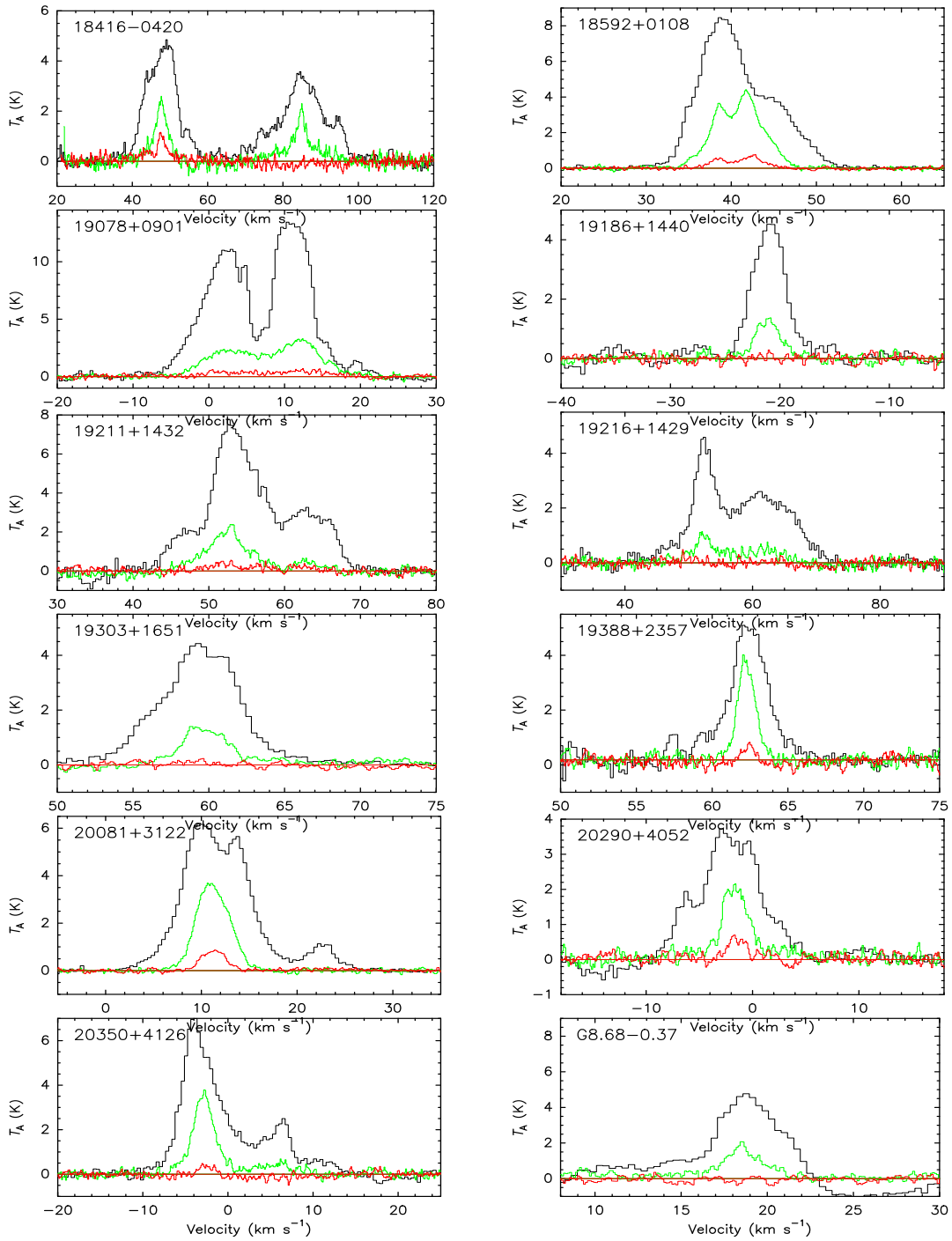


Fig. 3 Continued

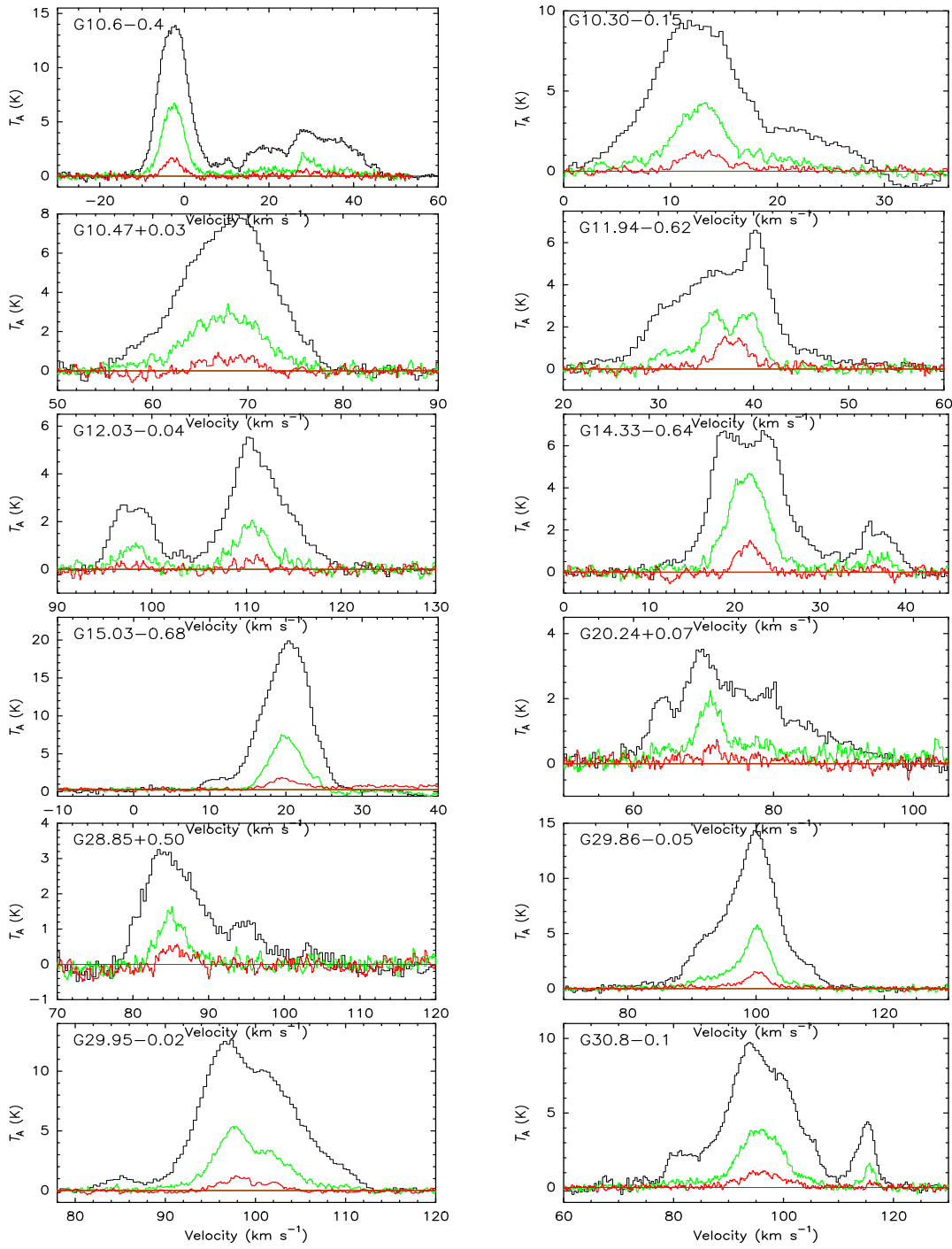


Fig. 3 Continued

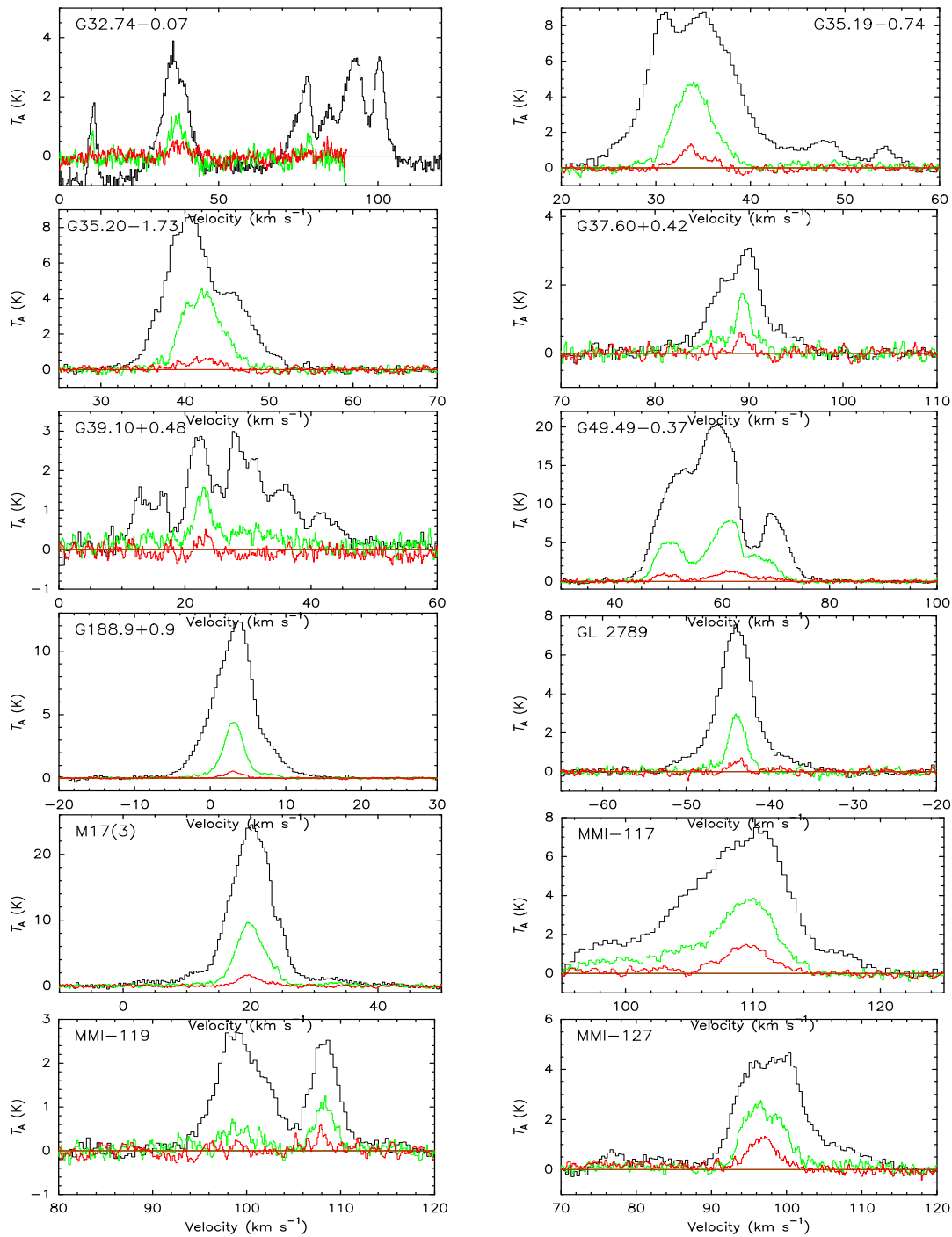


Fig. 3 Continued

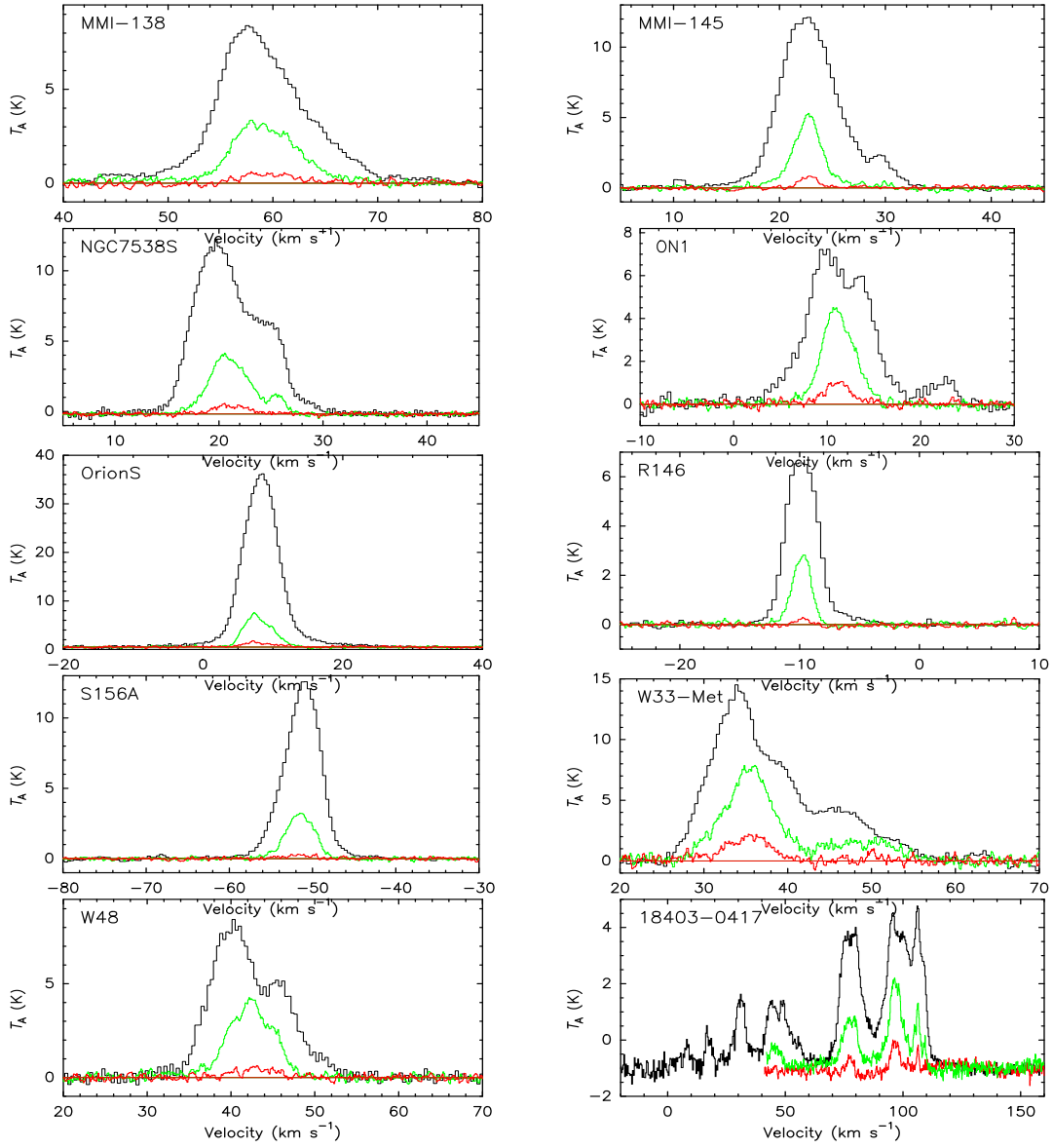


Fig.3 Continued

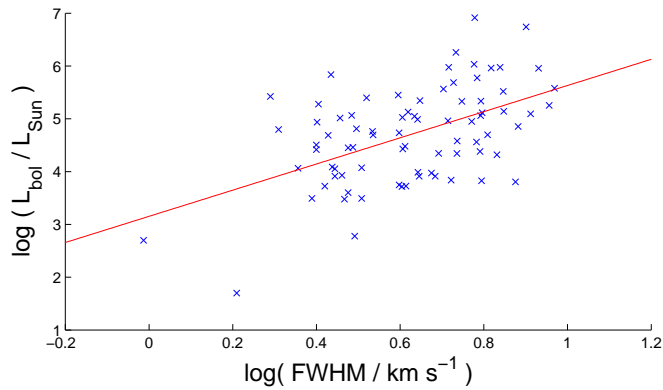


Fig.4 The bolometric luminosity (L_{bol}) versus ^{13}CO line width. The linear fit of L_{bol} and FWHM is: $\log(L_{bol}/L_{\odot}) = 2.5\log(\text{FWHM}/\text{km s}^{-1}) + 3.2$; the correlation coefficient $r=0.52$.

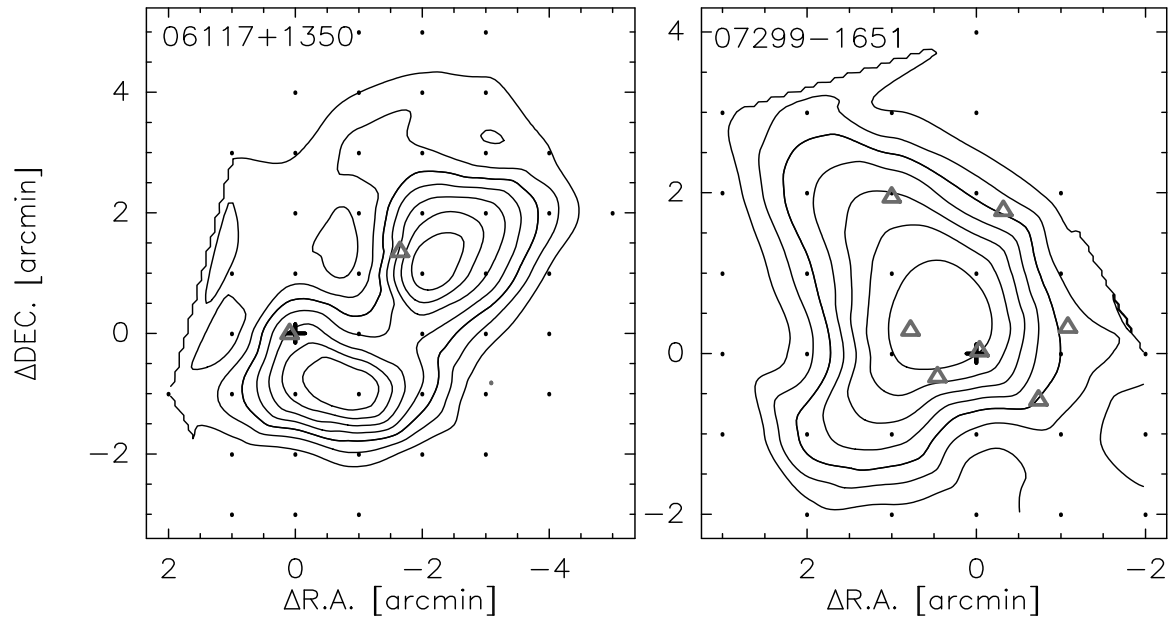


Fig. 5 The contours of the integrated intensities of ^{13}CO lines. Left: IRAS 06117+1350, Right: IRAS 07299-1651. The positions of IRAS sources are marked with "+" and the MSX sources are visualized with triangles.

Table 1 Parameters of all the sources surveyed

Name	IRAS No.	α (B1950)	δ (B1950)	l	b	log	log	Flux100	Type	Remark
		(h m s)	($^{\circ}$ ' '')	$^{\circ}$	$^{\circ}$	(F_{25} / F_{12})	(F_{60} / F_{12})	(Jy)		Ref.
(1)	(2)	(3)	(4)	(5)	(6)	(7)	(8)	(9)	(10)	(11)
02455+6034	02455+6034	02 45 30.1	+60 34 34.5	136.84	1.14	0.67	1.51	3.395×10^2	II	Szymczak et al. (2000)
05274+3345	05274+3345	05 27 27.59	+33 45 37.32	174.20	-0.08	1.00	1.81	9.057×10^2	II	Szymczak et al. (2000)
Orion's	05327-0529	05 32 44.8	-05 26 00.0	209.01	-19.41	1.03	2.15	2.448×10^1	I	Haschick et al. (1989)
06056+2131	06056+2131	06 05 40.9	+21 31 32.4	189.03	0.79	0.70	1.55	2.563×10^3	II	Szymczak et al. (2000)
G188.9+0.9	06058+2138	06 05 54.0	+21 39 09.4	188.95	0.89	1.00	1.83	1.666×10^3	I	Haschick et al. (1989)
06099+1800	06099+1800	06 09 57.90	+18 00 11.95	192.60	-0.05	0.54	1.47	5.285×10^3	II	Szymczak et al. (2000)
06117+1350	06117+1350	06 11 46.4	+13 50 32.7	196.45	-1.68	0.90	1.89	1.965×10^3	II	Szymczak et al. (2000)
07299-1651	07299-1651	07 29 55.0	-16 51 47.2	232.62	1.00	1.67	2.37	1.269×10^3	II	Szymczak et al. (2000)
G8.68-0.37	18032-2137	18 03 21.69	-21 37 42.27	8.68	-0.36	0.91	2.00	5.221×10^3	II	Caswell et al. (1993)
G10.47+0.03	18056-1952	18 05 40.54	-19 52 25.30	10.47	0.03	1.13	2.67	1.016×10^4	II	Caswell et al. (1993)
G10.30-0.15	18060-2005	18 05 57.93	-20 06 25.58	10.30	-0.15	0.87	1.63	1.201×10^4	I	Bachiller et al. (1990)
18067-1927	18067-1927	18 06 44.00	-19 27 02.90	10.96	0.02	0.87	2.10	1.292×10^3	II	Szymczak et al. (2000)
G10.6-0.4	18075-1956	18 07 30.6	-19 56 28.3	10.62	-0.38	0.80	2.61	2.137×10^4	I	Haschick et al. (1989)
G12.89+0.49	18089-1732	18 08 56.49	-17 32 14.46	12.89	0.49	0.87	2.31	3.148×10^3	I	Slysh et al. (1994)
G12.03-0.04	18090-1832	18 09 05.59	-18 32 44.17	12.02	-0.03	0.71	1.63	1.710×10^3	II	Caswell et al. (1993)
18092-1842	18092-1842	18 09 13.78	-18 42 19.77	11.90	-0.14	0.10	1.46	1.710×10^3	II	Szymczak et al. (2000)
G11.90-0.14	18092-1842	18 09 14.78	-18 42 20.84	11.90	-0.14	0.10	1.46	1.710×10^3	II	Caswell et al. (1993)
18108-1759	18108-1759	18 10 52.41	-17 59 35.92	12.71	-0.13	0.38	1.88	2.878×10^3	II	Szymczak et al. (2000)
G12.68-0.18	18112-1801	18 11 00.55	-18 02 47.51	12.68	-0.19	0.64	1.77	6.502×10^3	II	Caswell et al. (1993)
G11.94-0.62	18110-1854	18 11 04.4	-18 54 19.8	11.94	-0.62	1.21	2.19	4.930×10^3	I	Bachiller et al. (1990)
W33-Met	18108-1759	18 11 15.78	-17 56 52.62	12.80	-0.19	0.38	1.88	2.878×10^3	I	Haschick et al. (1990)
W33A	18117-1753	18 11 44.56	-17 52 55.71	12.91	-0.26	1.11	2.02	6.310×10^3	I	Haschick et al. (1989)
G12.91-0.26	18117-1753	18 11 45.36	-17 53 09.77	12.91	-0.27	1.11	2.02	6.310×10^3	II	Caswell et al. (1993)
18128-1640	18128-1640	18 12 51.82	-16 40 00.54	14.10	0.09	0.38	1.48	1.017×10^3	II	Szymczak et al. (2000)
18144-1723	18144-1723	18 14 29.81	-17 23 22.70	13.66	-0.60	0.56	1.61	1.137×10^3	II	Szymczak et al. (2000)
G14.33-0.64	18160-1647	18 16 00.9	-16 49 06.3	14.33	-0.65	0.94	2.24	2.819×10^3	I	Slysh et al. (1994)
M17(3)	18174-1612	18 17 31.03	-16 12 49.82	15.04	-0.67	0.89	1.71	6.589×10^4	I	Bachiller et al. (1990)
G15.03-0.68	18174-1612	18 17 31.72	-16 13 06.87	15.03	-0.68	0.89	1.71	6.589×10^4	II	Caswell et al. (1993)
18181-1534	18181-1534	18 18 06.73	-15 34 36.38	15.66	-0.50	-0.26	1.34	6.839×10^2	II	Szymczak et al. (2000)
G16.59-0.06	18182-1433	18 18 20.41	-14 33 18.33	16.59	-0.06	1.15	2.23	1.071×10^3	I	Slysh et al. (1994)
18220-1241	18220-1241	18 22 02.53	-12 41 00.36	18.66	0.03	1.06	2.23	1.095×10^3	II	Szymczak et al. (2000)
G20.24+0.07	18249-1116	18 24 57.15	-11 16 48.95	20.24	0.07	0.24	1.53	3.696×10^2	II	Caswell et al. (1993)
18249-1116	18249-1116	18 24 57.16	-11 16 41.95	20.24	0.07	0.24	1.53	3.696×10^2	II	Szymczak et al. (2000)
18278-1009	18278-1009	18 27 49.62	-10 09 19.38	21.56	-0.03	0.51	1.14	2.284×10^2	II	Szymczak et al. (2000)
G22.34-0.16	18297-0931	18 29 47.29	-09 31 25.86	22.34	-0.16	-0.26	0.48	2.823×10^2	II	Szymczak et al. (2002)
G22.43-0.17	18297-0931	18 29 59.07	-09 27 31.70	22.42	-0.17	-0.26	0.48	2.823×10^2	II	Caswell et al. (1993)
18316-0602	18316-0602	18 31 39.0	-06 02 07.8	25.65	1.05	0.78	1.62	2.136×10^3	II	Slysh et al. (1999)
18317-0859	18317-0859	18 31 44.83	-08 59 41.32	23.04	-0.34	0.18	1.77	1.940×10^2	II	Szymczak et al. (2000)
G23.01-0.41	18318-0901	18 31 56.26	-09 03 15.14	23.01	-0.41	0.70	2.50	4.393×10^3	II	Caswell et al. (1993)
G23.01-0.41	18318-0901	18 31 56.76	-09 03 18.18	23.01	-0.42	0.70	2.50	4.393×10^3	I	Slysh et al. (1994)
18322-0721	18322-0721	18 32 13.56	-07 21 42.32	24.54	0.31	-0.13	1.25	2.935×10^2	I	Szymczak et al. (2000)
18326-0751	18326-0751	18 32 38.38	-07 51 13.13	24.15	-0.01	0.79	2.09	5.740×10^2	I	Szymczak et al. (2000)
18335-0713	18335-0713	18 33 30.13	-07 13 09.83	24.81	0.10	0.96	1.98	6.936×10^3	II	Szymczak et al. (2000)
MMI-117	18335-0714	18 33 30.36	-07 14 41.97	24.79	0.08	0.96	1.98	6.936×10^3	I	Val'ts et al. (2007)
18353-0628	18353-0628	18 35 23.8	-06 28 07.0	25.70	0.03	0.81	1.59	2.435×10^3	II	Szymczak et al. (2000)
MMI-119	18379-0546	18 37 58.3	-05 46 28.0	26.61	-0.22	0.91	1.86	5.343×10^2	I	Val'ts et al. (2007)
MMI-121	18391-0504	18 39 11.55	-05 04 24.47	27.37	-0.16	-0.15	0.59	1.633×10^3	I	Val'ts et al. (2007)
G28.85+0.50	18396-0322	18 39 35.13	-03 27 23.91	28.85	0.50	0.37	1.13	4.073×10^2	II	Błazkiewicz & Kus (2004)

Table 1 Continued.

Name	IRAS No.	α (B1950)	δ (B1950)	l	b	log	log	Flux100	Type	Remark
		(h m s)	($^{\circ}$ ' ")	$^{\circ}$	$^{\circ}$	(F_{25} / F_{12})	(F_{60} / F_{12})	(Jy)		Ref.
(1)	(2)	(3)	(4)	(5)	(6)	(7)	(8)	(9)	(10)	(11)
G28.15+0.00	18402-0418	18 40 02.45	-04 18 20.91	28.15	0.00	0.33	2.80	5.877×10^2	II	Szymczak et al. (2002)
G28.53+0.12	18403-0354	18 40 19.50	-03 55 00.11	28.53	0.12	-0.39	1.04	2.437×10^2	II	Szymczak et al. (2002)
18403-0417	18403-0417	18 40 19.58	-04 17 01.13	28.20	-0.05	0.91	1.86	3.937×10^3	II	Szymczak et al. (2000)
18416-0420	18416-0420	18 41 39.81	-04 20 59.88	28.29	-0.38	0.95	1.57	4.358×10^3	II	Szymczak et al. (2000)
G28.83-0.25	18421-0349	18 42 11.63	-03 49 01.14	28.83	-0.25	1.04	2.11	1.877×10^3	II	Caswell et al. (1993)
G29.86-0.05	18434-0242	18 43 24.69	-02 48 40.33	29.86	-0.05	0.89	1.54	1.167×10^4	II	Szymczak et al. (2002)
G29.95-0.02	18434-0242	18 43 27.0	-02 42 45.5	29.95	-0.02	0.89	1.54	1.167×10^4	II	Caswell et al. (1993)
G30.69-0.06	18449-0207	18 44 58.94	-02 04 27.03	30.70	-0.06	0.64	2.26	4.025×10^3	I	Slysh et al. (1994)
MMI-125	18449-0207	18 44 58.96	-02 04 26.97	30.70	-0.06	0.64	2.26	4.025×10^3	I	Val'ts et al. (2007)
MMI-127	18449-0115	18 44 59.2	-01 16 10.6	31.41	0.31	1.11	2.43	2.815×10^3	I	Val'ts et al. (2007)
G30.8-0.1	18449-0158	18 45 11.06	-01 57 56.89	30.82	-0.06	0.80	1.81	1.908×10^4	I	Haschick et al. (1989)
G31.28+0.06	18456-0129	18 45 36.80	-01 29 51.71	31.28	0.06	1.26	2.34	3.693×10^3	II	Caswell et al. (1993)
18456-0129	18456-0129	18 45 39.70	-01 29 48.92	31.29	0.05	1.26	2.34	3.693×10^3	II	Szymczak et al. (2000)
G32.74-0.07?	18487-0015	18 48 47.51	-00 15 48.25	32.74	-0.08	0.36	1.89	1.071×10^3	II	Caswell et al. (1993)
18497+0022	18497+0022	18 49 46.43	+00 22 05.59	33.41	-0.002	0.37	1.61	2.064×10^3	II	Szymczak et al. (2000)
G33.74-0.15	18509+0035	18 50 53.88	+00 35 14.80	33.74	-0.15	0.19	2.68	1.757×10^2	II	Szymczak et al. (2002)
G33.64-0.21	18509+0027	18 50 55.54	+00 28 11.68	33.64	-0.21	-0.09	0.95	5.536×10^2	II	Blaszkiewicz & Kus. (2004)
G35.05-0.52	18546+0139	18 54 37.21	+01 35 01.02	35.05	-0.52	-0.26	0.19	1.487×10^3	I	Bachiller et al. (1990)
G35.79-0.17	18547+0223	18 54 45.12	+02 23 41.49	35.79	-0.17	0.11	1.67	2.739×10^2	II	Szymczak et al. (2002)
G35.19-0.74	18556+0136	18 55 40.43	+01 36 33.55	35.20	-0.74	1.71	2.66	1.124×10^3	II	Caswell et al. (1993)
G37.60+0.42	18559+0416	18 55 59.7	+04 16 26.3	37.60	0.42	0.18	1.36	2.451×10^2	II	Szymczak et al. (2002)
G37.02-0.03	18566+0330	18 56 30.24	+03 33 30.11	37.02	-0.03	-0.24	0.24	1.553×10^2	II	Szymczak et al. (2002)
18577+0358	18577+0358	18 57 45.20	+03 58 19.84	37.53	-0.11	0.86	1.88	1.867×10^3	II	Blaszkiewicz & Kus. (2004)
G39.10+0.48	18585+0538	18 58 32.19	+05 38 09.59	39.10	0.48	-0.03	1.57	1.734×10^2	II	Szymczak et al. (2002)
G35.20-1.73	18592+0108	18 59 12.72	+01 09 14.56	35.20	-1.73	0.95	1.95	1.396×10^4	II	Caswell et al. (1993)
W48	18592+0108	18 59 13.82	+01 09 13.49	35.20	-1.74	0.95	1.95	1.396×10^4	I	Haschick et al. (1989)
18592+0108	18592+0108	18 59 14.6	+01 08 46.4	35.20	-1.75	0.95	1.95	1.396×10^4	II	Szymczak et al. (2000)
19031+0621	19031+0621	19 03 09.87	+06 21 31.12	40.27	-0.20	1.26	2.48	3.658×10^2	II	Szymczak et al. (2000)
19078+0901	19078+0901	19 07 51.8	+09 01 10.5	43.17	0.00	1.01	1.86	3.615×10^4	II	Szymczak et al. (2000)
MMI-134	19092+0841	19 09 14.96	+08 41 34.73	43.04	-0.45	0.51	1.82	5.105×10^2	I	Val'ts et al. (2007)
19095+0930	19095+0930	19 09 30.29	+09 30 41.71	43.79	-0.13	1.39	2.51	2.744×10^3	II	Szymczak et al. (2000)
G43.8-0.1	19099-0934	19 09 31.26	-09 30 51.10	26.83	-8.88	0.14	0.26	2.480×10^0	I	Haschick et al. (1989)
MMI-138	19120+1103	19 12 04.6	+11 04 22.5	45.47	0.05	0.91	1.83	7.890×10^3	I	Val'ts et al. (2007)
19186+1440	19186+1440	19 18 39.8	+14 40 58.0	49.41	0.33	0.53	1.76	1.710×10^2	II	Blaszkiewicz & Kus. (2004)
19211+1432	19211+1432	19 21 10.45	+14 32 18.69	49.57	-0.27	0.41	1.42	6.230×10^1	II	Szymczak et al. (2000)
MMI-143	19213+1424	19 21 19.66	+14 25 14.97	49.49	-0.36	1.01	-1.95	2.676×10^4	I	Val'ts et al. (2007)
G49.49-0.37	19213+1424	19 21 22.31	+14 25 07.88	49.49	-0.37	1.01	-1.95	2.676×10^4	II	Caswell et al. (1993)
19216+1429	19216+1429	19 21 37.3	+14 29 51.9	49.59	-0.39	0.96	1.72	1.586×10^3	II	Szymczak et al. (2000)
19303+1651	19303+1651	19 30 20.3	+16 51 04.5	52.66	-1.09	0.64	1.77	1.238×10^2	II	Blaszkiewicz & Kus. (2004)
19388+2357	19388+2357	19 38 52.7	+23 57 35.7	59.83	0.67	0.93	2.30	4.334×10^2	II	Slysh et al. (1999)
MMI-145	19410+2336	19 41 04.3	+23 36 42.0	59.78	0.06	0.88	1.83	1.631×10^3	I	Val'ts et al. (2007)
20081+3122	20081+3122	20 08 09.9	+31 22 38.6	69.54	-0.98	1.72	3.11	3.119×10^3	II	Szymczak et al. (2000)
ONI	20081+3122	20 08 09.92	+31 22 41.59	69.54	-0.98	1.72	3.11	3.119×10^3	I	Haschick et al. (1990)
20290+4052	20290+4052	20 29 03.1	+40 52 15.0	79.74	0.99	0.98	2.05	1.367×10^2	II	Blaszkiewicz & Kus. (2004)
20350+4126	20350+4126	20 35 04.9	+41 26 02.3	80.87	0.42	1.07	1.95	3.272×10^3	II	Slysh et al. (1999)
21074+4949	21074+4949	21 07 28.47	+49 49 46.09	90.92	1.51	1.02	2.25	7.148×10^2	II	Szymczak et al. (2000)
GL2789	21381+5000	21 38 11.3	+50 00 45.3	94.60	-1.80	0.28	0.51	4.546×10^2	II	Slysh et al. (1999)
R146	21426+6556	21 42 40.1	+65 52 56.9	105.47	9.83	-0.17	0.74	2.119×10^1	I	Kalenskii et al. (1994)
S156A	23030+5958	23 03 05.03	+59 58 09.38	110.11	0.04	0.81	1.59	1.833×10^3	II	Bachiller et al. (1990)

Table 2 Sources with resolved components

Name	T_A^* (K)	V_{LSR} ($km\ s^{-1}$)	FWHM ($km\ s^{-1}$)	R (kpc)	D (kpc)	L_{bol} (L_{\odot})	T_{ex} (K)	τ_{13}	$N(^{13}CO)$ ($10^{16}\ cm^{-2}$)	$N(H_2)$ ($10^{22}\ cm^{-2}$)	Pro
(1)	(2)	(3)	(4)	(5)	(6)	(7)	(8)	(9)	(10)	(11)	(12)
02455+6034	1.3(9)	-42.51(0)	2.78(1)	12.19	4.52	1.1×10^4	16.04	0.22	0.9	0.8	d
	1.2(8)	-37.40(0)	2.78(3)	11.62	3.86	8.2×10^3	13.22	0.27	0.8	0.7	d
OrionS	6.5(1)	7.80(4)	4.73(7)	9.39	1.06	9.4×10^3	47.92	0.26	14.2	1.2	e
06056+2131	5.8(0)	2.66(9)	2.99(5)	9.38	0.89	4.0×10^3	19.99	0.81	5.3	4.7	
G188.9+0.9	4.4(4)	3.06(8)	3.22(6)	9.52	1.03	3.1×10^3	18.78	0.61	3.8	3.4	a
06117+1350	2.1(5)	17.80(1)	3.42(8)	12.25	3.86	5.8×10^4	20.52	0.22	1.7	1.6	f
07299-1651	3.4(7)	16.50(3)	2.89(3)	9.57	1.62	8.5×10^3	15.04	0.64	2.4	2.1	a
G10.47+0.03	2.8(1)	67.65(2)	9.31(2)	3.08	5.69	3.8×10^5	13.18	0.61	5.8	5.2	g
G10.6-0.4	6.5(3)	-2.65(0)	6.00(7)	9.26	17.48	8.2×10^6	20.99	0.89	12.7	11.4	g
	1.4(3)	29.08(3)	5.05(9)	4.92	3.69	3.7×10^5	7.77	0.69	8.5	7.6	d
G11.94-0.62	2.5(7)	35.78(9)	2.86(1)	4.72	3.94	1.0×10^5	8.71	1.39	2.0	1.8	c,g
	2.6(6)	39.48(0)	3.05(2)	4.5	4.17	1.2×10^5	7.51	4.45	5.4	4.9	g
18144-1723	0.5(0)	16.73(0)	6.23(0)	6.45	2.13	6.7×10^3	9.92	0.13	0.5	0.5	g
	0.6(3)	41.65(7)	6.18(8)	4.68	4.04	2.4×10^4	6.88	0.32	0.7	0.6	
	1.4(6)	48.15(8)	2.99(0)	4.36	4.39	2.8×10^4	7.15	0.89	1.0	0.9	
G14.33-0.64	4.6(3)	21.52(3)	5.44(6)	6.1	2.51	2.2×10^4	12.54	1.61	8.3	7.4	g
G15.03-0.68	8.1(9)	20.00(1)	5.34(6)	6.31	2.29	4.9×10^5	32.03	0.61	17.0	15.2	e,g
18181-1534	1.1(7)	-5.44(3)	3.31(2)	9.54	17.44	2.5×10^5	7.8	0.52	0.7	0.7	g
	2.6(2)	16.90(6)	2.45(5)	6.65	1.94	3.1×10^3	10.13	0.94	1.5	1.4	e
18316-0602	3.4(7)	42.10(5)	4.09(5)	5.9	3.06	3.0×10^4	11.16	1.21	3.8	3.4	e
	1.1(0)	47.59(4)	6.06(9)	5.66	3.36	3.6×10^4	8.01	0.46	1.2	1.1	g
18353-0628	1.3(3)	54.12(6)	5.45(8)	5.41	3.7	3.8×10^4	8.46	0.52	1.4	1.2	g
	1.3(4)	97.32(5)	5.18(4)	4.15	5.75	9.2×10^4	9.31	0.44	1.3	1.1	f
	0.6(4)	105.88(4)	4.03(7)	3.97	6.19	1.1×10^5	6.09	0.43	0.5	0.4	g
MMI-119	0.4(5)	99.18(8)	4.04(0)	4.18	5.87	2.7×10^4	6.35	0.26	0.3	0.3	g
	1.0(2)	108.28(2)	2.51(4)	3.99	6.41	3.2×10^4	6.18	0.77	0.6	0.5	g
G29.95-0.02	4.6(0)	98.68(2)	8.53(9)	4.43	6.1	9.0×10^5	17.75	0.71	10.6	9.5	d
MMI-127	2.4(9)	96.94(9)	6.25(6)	4.56	6.17	1.3×10^5	8.53	1.39	4.3	3.8	e
G32.74-0.07	0.8(7)	10.29(3)	0.97(5)	7.92	0.7	0.5×10^3	6.15	0.62	0.2	0.2	
	1.2(9)	36.96(6)	5.27(2)	6.51	2.54	6.9×10^3	7.59	0.64	1.4	1.2	g
	0.7(0)	78.24(1)	2.51(4)	5.1	4.94	2.6×10^4	5.56	0.61	0.4	0.3	g
G37.60+0.42	1.5(0)	89.37(2)	2.27(0)	5.07			6.55	1.23	0.9	0.8	c
18592+0108	2.3(4)	39.35(4)	2.54(0)	6.51	2.66	1.9×10^5	13.53	0.46	1.2	1.1	
	3.8(6)	42.89(3)	4.44(0)	6.37	2.87	2.2×10^5	13.53	0.92	4.4	3.9	
19078+0901	3.0(1)	12.04(5)	6.78(8)	7.97	0.76	2.0×10^4	21.05	0.32	5.1	4.6	e
	2.3(1)	2.78(8)	7.96(5)	8.47	12.35	5.5×10^6	16.96	0.32	4.0	3.6	g
MMI-138	3.1(0)	59.12(4)	7.02(8)	6.19	4.71	3.3×10^5	13.13	0.7	5.0	4.5	f
19186+1440	1.2(7)	-21.10(7)	2.68(5)	9.93	13.08	4.9×10^4	8.89	0.45	0.6	0.6	g
19216+1429	0.8(5)	52.39(3)	4.38(8)	6.5	4.88	9.8×10^4	7.79	0.35	0.7	0.6	g
	0.4(8)	61.16(1)	8.16(4)	6.24			6.32	0.28	0.7	0.6	
19303+1651	1.2(8)	59.73(6)	3.96(1)	6.36			8.76	0.46	14.3	12.7	b,i
19388+2357	3.0(3)	34.50(6)	2.74(5)	7.26			8.23	3.34	4.3	3.8	
MMI-145	4.9(2)	22.67(2)	3.22(4)	7.68	2.05	1.2×10^4	18.37	0.74	4.4	4.0	a
20081+3122	4.2(8)	11.09(7)	4.02(3)	8.17	1.13	5.2×10^3	11.77	1.64	5.6	5.0	
20290+4052	2.0(1)	-1.62(4)	2.93(8)	8.7	3.91	3.0×10^3	9.12	0.99	1.6	1.4	g
20350+4126	3.5(0)	-2.87(0)	3.13(0)	8.75	3.83	6.5×10^4	13.69	0.96	3.3	3.0	c
GL2789	2.8(7)	-43.86(8)	2.52(5)	10.89	6.16	8.6×10^4	15	0.6	1.9	1.7	c
R146	3.0(0)	-9.73(9)	1.62(9)	9.07			15.38	0.61	1.3	1.2	
S156A	3.0(6)	-51.51(2)	4.16(0)	11.63	5.54	1.3×10^5	27.38	0.26	4.3	3.8	f

Table 2 Continued.

Name	T_A^* (K)	V_{LSR} ($km\ s^{-1}$)	FWHM ($km\ s^{-1}$)	R (kpc)	D (kpc)	L_{bol} (L_\odot)	T_{ex} (K)	τ_{13}	$N(^{13}CO)$ ($10^{16}\ cm^{-2}$)	$N(H_2)$ ($10^{22}\ cm^{-2}$)	Pro
(1)	(2)	(3)	(4)	(5)	(6)	(7)	(8)	(9)	(10)	(11)	(12)
05274+3345	5.1(9)	-3.66(5)	2.63(6)	10.41	1.92	5.3×10^3	16.42	1	4.0	3.6	
06099+1800	6.9(1)	7.15(2)	3.07(6)	10.21	1.74	2.9×10^4	29.03	0.56	7.5	6.7	
G8.68-0.37	1.4(2)	18.53(9)	2.04(6)	5.44	3.12	6.3×10^4	9.79	0.43	0.5	0.5	
	3.8(3)	36.65(8)	7.04(4)	3.98	4.64	1.4×10^5	13.81	0.87	6.7	6.1	e
G10.30-0.15	3.7(1)	12.86(8)	5.90(6)	6.43	2.12	8.9×10^4	14.94	0.71	5.4	4.8	b
G12.03-0.04	0.9(3)	98.05(1)	3.43(3)	2.62	6.38	5.0×10^4	6.77	0.53	0.6	0.6	g
	1.7(3)	110.61(5)	3.96(9)	2.41	6.69	5.4×10^4	9.48	0.58	1.4	1.2	g
W33-Met	6.9(7)	35.43(3)	6.44(0)	4.89	3.78	5.0×10^4	19.27	1.2	15.7	14.0	g
	1.1(2)	48.56(1)	7.62(6)	4.2	4.53	7.2×10^4	8.61	0.41	1.5	1.4	
M17(3)	9.1(3)	19.98(6)	5.41(0)	4.12	4.42	1.8×10^6	32.58	0.69	20.1	18.0	e
G20.24+0.07	1.6(2)	71.06(4)	4.39(8)	4.35	4.77	9.7×10^3	6.65	1.35	2.0	1.8	a
MM1-117	3.4(9)	109.22(3)	6.20(4)	3.83	6.32	1.2×10^5	11.64	1.1	5.7	5.0	c
G28.85+0.50	1.4(0)	85.13(2)	4.42(6)	4.68	5.2	8.2×10^3	6.9	0.92	1.4	1.3	e
18416-0420	2.1(2)	47.61(3)	4.31(8)	5.83	3.26	1.1×10^5	8.28	1.11	2.2	2.0	c
	1.5(7)	84.78(5)	3.94(3)	4.65	5.17	2.8×10^5	6.3	1.59	1.9	1.7	a
G29.86-0.05	4.9(7)	99.89(3)	5.98(3)	2.24	6.67	1.1×10^6	18.77	0.72	8.3	7.5	c
G30.8-0.1	3.6(8)	95.93(4)	9.04(0)	4.55	5.99	1.8×10^5	14.82	0.71	8.2	7.3	g,a
	1.3(9)	115.63(0)	1.95(7)	4.14			8.46	0.55	0.5	0.5	c
G35.19-0.74	4.5(9)	33.88(3)	4.92(2)	6.75	2.31	2.2×10^4	13.24	1.34	6.8	6.1	g
G39.10+0.48	1.2(4)	22.96(1)	3.10(0)	7.36	1.55	0.6×10^3	6.65	0.84	0.9	0.8	e,g
G35.20-1.73	4.2(6)	41.99(4)	5.59(8)	6.41	2.82	2.1×10^5	13.83	1.04	6.5	5.8	f
W48	3.8(6)	42.37(7)	6.21(5)	6.39	2.84	2.2×10^5	13.34	0.95	6.2	5.6	d,f
19211+1432	2.0(4)	52.32(3)	7.51(4)	6.5	4.85	6.4×10^3	11.96	0.47	3.1	2.8	c,e
	0.5(5)	63.10(1)	4.83(4)	6.19			7.01	0.26	0.5	0.4	
G49.49-0.37	5.2(5)	50.31(9)	6.08(8)	6.56	4.37	5.9×10^5	15.62	1.14	9.7	8.6	g
	7.6(0)	60.61(9)	6.90(8)	6.26			28.42	0.66	19.0	17.0	g
	2.5(3)	68.13(2)	5.20(8)	6.05			13.14	0.53	2.8	2.5	g
ON1	4.3(3)	11.13(4)	4.11(5)	8.17	1.14	5.3×10^3	11.9	1.63	5.8	5.2	e
NGC7538S	5.0(0)	-56.14(8)	6.57(9)	12.05	5.98	9.1×10^5	27.4	0.48	12.2	11.0	f
	1.4(7)	-48.95(9)	2.72(0)	11.47	5.19	6.9×10^5	15.19	0.26	0.9	0.8	g

Table 3 Physical parameters of the ^{13}CO Molecular Cores

Name	α (B1950) (h m s)	δ (B1950) ($^\circ\ ' ''$)	V_{LSR} ($km\ s^{-1}$)	FWHM ($km\ s^{-1}$)	D (kpc)	T_{ex} (K)	R (pc)	$N(H_2)$ ($10^{22}\ cm^{-2}$)	M_{core} (M_\odot)	M_{vir} (M_\odot)
06117+1350-SE	06 11 46.4	+13 50 32.7	16.48(2)	3.34(9)	3.86	18.47	1.45	2.1	4.0×10^3	3.4×10^3
06117+1350-NW	06 11 46.4	+13 50 32.7	16.68(3)	2.95(7)	3.86	17.29	1.42	2.0	3.6×10^3	2.6×10^3
07299-1651	07 29 55.0	-16 51 47.2	16.50(3)	2.89(3)	1.62	15.04	0.79	2.2	1.2×10^3	1.4×10^3

07299-1651 $^{13}\text{CO}(J=1-0)$, $V_{\text{LSR}} = 11.08 \sim 24.14 \text{ km s}^{-1}$

